Available online at www.sciencedirect.com

ScienceDirect

Ceramics International 39 (2013) 9721–9726

CERAMICS INTERNATIONAL

www.elsevier.com/locate/ceramint

Short communication

Mechanical properties and consolidation of binderless nanostructured (Ti,Cr)C from mechanochemically-synthesized powder by high-frequency induction heating sintering

In-Jin Shon[a,*], Hyun-Su Oh[a], Jae-Won Lim[b], Hanjung Kwon[b]

[a]*Division of Advanced Materials Engineering and the Research Center of Hydrogen and Fuel Cell, Engineering College, Chonbuk National University, Jeonju 561-756, Republic of Korea*

[b]*Minerals and Materials Processing Division, Korea Institute of Geoscience, Mining and Materials Resources, Daejeon, Republic of Korea*

Received 21 March 2013; received in revised form 3 April 2013; accepted 15 April 2013
Available online 21 April 2013

Abstract

Solid-solution nanocrystalline powder, (Ti,Cr)C, was prepared via high-energy milling of Ti alloys with graphite resulting in the B1 structure (NaCl-like structure) phase. The synthesis process was investigated in terms of the phase evolution by analyzing XRD data. The rapid sintering of nanostuctured hard (Ti,Cr)C materials was performed by a high-frequency induction-heating sintering process. This process allows quick densification to near theoretical density and inhibits grain growth. A dense, nanostructured (Ti,Cr)C hard material with a relative density of up to 97% was produced by simultaneous application of 80 MPa and an induced current of 15 kW for 2 min. The microstructure and mechanical properties of the resulting binderless (Ti,Cr)C were investigated.

Keywords: A. Sintering; C. Fracture toughness; C. Mechanical properties; Nanostructured material; Powder metallurgy

1. Introduction

Some of the attractive properties of titanium carbide include its hardness, low density, and relatively high thermal and electrical conductivity. TiC is also very stable, with a melting temperature of 2727 K, and does not undergo phase transformations in this range. These properties have led to TiC being used extensively in cutting tools and as a composite abrasive material with a binder metal such as Ni. The low toughness of titanium carbide, however, leads to structural failures during high-speed machining, resulting in a shortened tool life [1,2]. One approach, commonly utilized to improve fracture toughness, has been to form solid solution carbide and make nanostructured materials [3].

Nanocrystalline materials have recently received significant attention in the area of advanced engineering materials due to their improved physical and mechanical properties [4,5]. Nanomaterials possess high strength and hardness, as well as excellent ductility and toughness, which are ideal qualities for applied uses [6,7]. Recently, nanocrystalline powders have been developed via the spray conversion process (SCP), a thermochemical and thermomechanical process, co-precipitation, and high-energy milling [8–10]. The sintering temperature of high-energy mechanically-milled powder is lower than that of unmilled powder due to the increased reactivity, internal and surface energies, and surface area of the milled powder, which contribute to its so-called mechanical activation [11–13]. The final grain size in sintered materials, however, is significantly larger than in pre-sintered powders due to rapid grain growth during the conventional sintering process. Grain particles with an initial size of 100 nm can rapidly reach 2 μm or larger during conventional sintering [14]. Controlling grain growth during the sintering process is, therefore, key to the commercial success of nanostructured materials. The high-frequency induction-heated sintering (HFIHS) method, which enables formation of dense materials within 2 min, has been proven effective in achieving this goal [15–17]. In addition,

*Corresponding author. Tel.: +82 63 270 2381; fax: +82 63 270 2386.
E-mail address: ijshon@chonbuk.ac.kr (I.-J. Shon).

0272-8842/$ - see front matter © 2013 Elsevier Ltd and Techna Group S.r.l. All rights reserved.
http://dx.doi.org/10.1016/j.ceramint.2013.04.053

spark plasma formed between the powder particles enhances both the distortion energy of the particles and the rate of the diffusion between the particles [18–21].

In this work, the synthesis of (Ti,Cr)C using high-energy ball milling and sintering of (Ti,Cr)C was investigated using the HFIHS method which removed the need for binders. The goal of this research is to produce a dense, fine-grained, binderless (Ti,Cr)C hard material. The microstructures and mechanical properties specific to binderless (Ti,Cr)C were also studied.

2. Experimental procedure

(Ti,Cr)C powder was produced using Ti–Cr alloy powders (99.9% purity, 180 μm average particle size, Ti:Cr=80:20 wt%). These were mixed with graphite to attain target compositions equivalent to $(Ti_{0.81}Cr_{0.19})C$. The powders were subjected to high-energy ball milling using a planetary mill (Model Pulverisette 5, Fritsch, Germany). Tungsten carbide balls were mixed with Ti–Cr alloy and graphite at ball-to-powder weight ratio of 20:1. The milling times were varied from 10 h to 20 h. A stainless steel bowl was used, and all milling was conducted at a speed of 250 RPM. The synthesized (Ti,Cr)C powders were annealed at 1200 °C for 2 h in a graphite furnace under vacuum.

The powders were placed in a graphite die (outside diameter, 35 mm; inside diameter, 10 mm; height, 40 mm) and then introduced into a high-frequency induction heating sintering (HFIHS) apparatus shown schematically in Fig. 1. The HFIHS apparatus includes a 15 kW power supply, which directs an induced current through the sample, as well as loads the sample with 50 kN of uniaxial pressure. The system was first evacuated and a uniaxial pressure of 80 MPa was applied. An induced current was then activated and maintained until the densification rate was negligible, as indicated by the real-time output of sample shrinkage. Shrinkage was measured using a linear gauge to determine the vertical displacement. Temperatures were measured with a pyrometer, which was focused on the surface of the graphite die. At the end of the process, the induced current was turned off and the sample cooled to room temperature. This process was carried out under a 5.33 Pa vacuum.

The relative density of the sintered sample was measured using the Archimedes method. Microstructural information was obtained from product samples, which had been polished and etched using Murakami's reagent (10 g potassium ferricyanide, 10 g NaOH, and 100 mL water) for 1–2 min at room temperature. Compositional and microstructural analyses of the products were made through X-ray diffraction (XRD), scanning electron microscopy (SEM) with energy dispersive spectroscopy (EDS), and field emission scanning electron microscopy (FE-SEM). The Vickers hardness was measured by performing indentations at a load of 30 kg_f and a dwell time of 15 s.

The grain size of the (Ti,Cr)C was calculated from the full width at half-maximum (FWHM) of the diffraction peak using the formula of Suryanarayana and Norton [22]:

$$B_r(B_{crystalline} + B_{strain})\cos\theta = kl/L + \eta \sin\theta \quad (1)$$

where B_r is the full width at half-maximum (FWHM) of the diffraction peak after instrumental correction; $B_{crystalline}$ and B_{strain} are the FWHM caused by small grain size and internal stress, respectively; k is a constant and has a value of 0.9; λ is the wavelength of the X-ray radiation; L and η are the grain size and internal strain, respectively; and θ is the Bragg angle. The parameters B and B_r follow Cauchy's form with the relationship $B=B_r+B_s$, where B and B_s are the FWHM of the broadened Bragg peaks and the standard sample's Bragg peaks, respectively.

3. Results and discussion

Fig. 2 shows XRD results pertaining to the milled powders following the high-energy milling of the mixtures of Ti–Cr

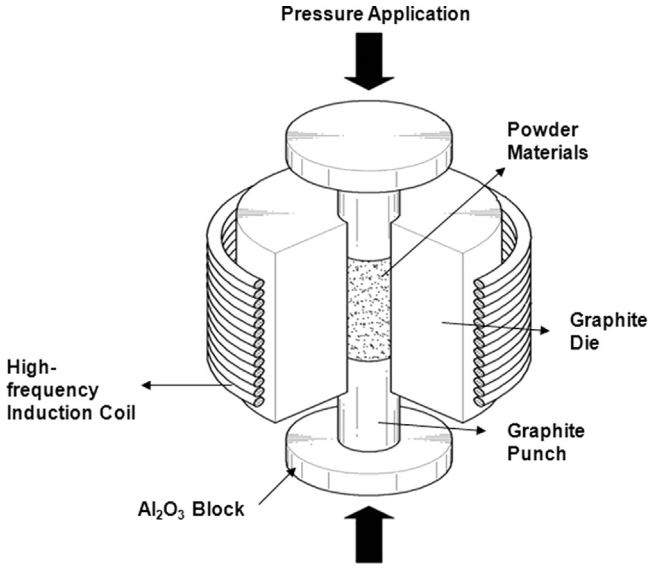

Fig. 1. Schematic diagram of the high-frequency induction heating sintering (HFIHS) apparatus.

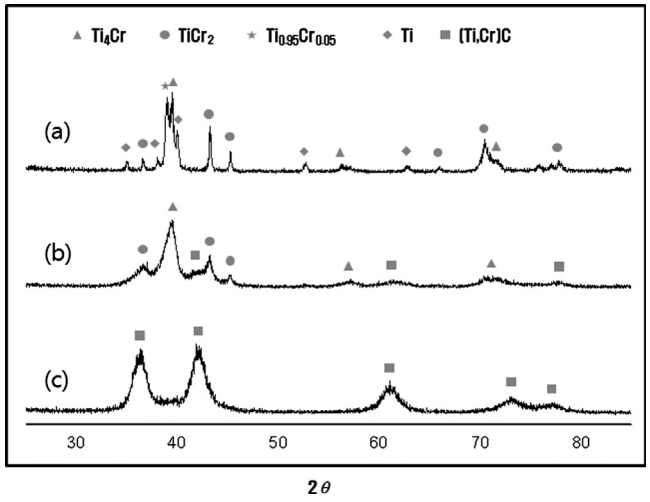

Fig. 2. X-ray diffraction patterns of the milled Ti–Cr+graphite powder: (a) 0 h, (b) 10 h, and (c) 20 h.

alloy and graphite. The Ti–Cr alloy consists of pure Ti, $Ti_{0.95}Cr_{0.05}$, Ti_4Cr, and $TiCr_2$. The peaks of the metallic phases broadened after 10 h of milling due to the strain and size reduction. The carbide phase from the reaction of Ti with amorphous graphite was noted. At a milling time of 20 h, only the (Ti,Cr)C phase with B1, a NaCl-like structure, was observed. SEM images of raw, milled powder are shown in Fig. 3. Raw, un-milled powder contains angularly-shaped particles, whereas the particles in the milled powder were round, due to refinement from milling. Fig. 4 shows a plot of $B_r(B_{crystalline}+B_{strain})\cos\theta$ versus $\sin\theta$ (Eq. (1)) in the formula of Suryanarayana and Norton [22] used to calculate particle size. The average grain size of the (Ti,Cr)C, calculated from the XRD data, was approximately 34 nm for samples with milling times of 20 h. Fig. 5 shows variations in shrinkage displacement and temperature as a function of heating time, with 80% of the total output power capacity (15 kW) during the sintering of (Ti,Cr)C which was synthesized by high-energy ball milling at a pressure of 80 MPa. The application of the induced current resulted in shrinkage due to consolidation. As the induced current was applied, shrinkage displacement initially showed a rapid increase, followed by a slow increase up to 1500 °C, with another rapid increase above this temperature. The high-energy ball milling affected the rate of densification and the final density. The high-energy ball milling treatment allows for the control of compound formation by fixing the reactant powder microstructure. Indeed, the high-energy ball milling produces fine crystallites, and high strain and defect densities. Therefore, the consolidation temperature decreases with milling time, because the driving force for sintering and the contact points of the powders for atomic diffusion increase. Fig. 6 shows the XRD pattern of (Ti,Cr)C sintered at 1650 °C. All peaks were from (Ti,Cr)C. A plot of $B_r(B_{crystalline}+B_{strain})\cos\theta$ versus $\sin\theta$ using the formula of Suryanarayana and Norton [22] (Eq. (1)) is shown in Fig. 7. The average grain sizes of the (Ti,Cr)C were calculated from the XRD data to be around 150 nm for samples with milling times of 20 h, and the corresponding densities were approximately 97%. Thus, the average grain size of the sintered (Ti,Cr)C was not significantly larger than that of the initial powder, indicating the absence of any appreciable grain growth during sintering. The retention of the grain size is attributed to a high heating rate, in conjunction with relatively short term exposure of the powders to high temperature. The SEM images of (Ti,Cr)C, sintered at 1650 °C from a powder milled for 20 h, show a dense microstructure and microstructures which consist of nano-grains, as shown in Fig. 8a and b, respectively.

The role of the current (resistive or inductive) in sintering and/or synthesis has been the focus of several studies, with the aim of providing an explanation for the known enhancement characteristic of sintering, as well as that of the subsequent products; however, no consensus has yet been reached. Theories include the effect which can be explained in terms of a fast heating rate due to Joule heating, the presence of plasma in the pores separating powder particles [18], and the intrinsic contribution of the current to mass transport [19–21].

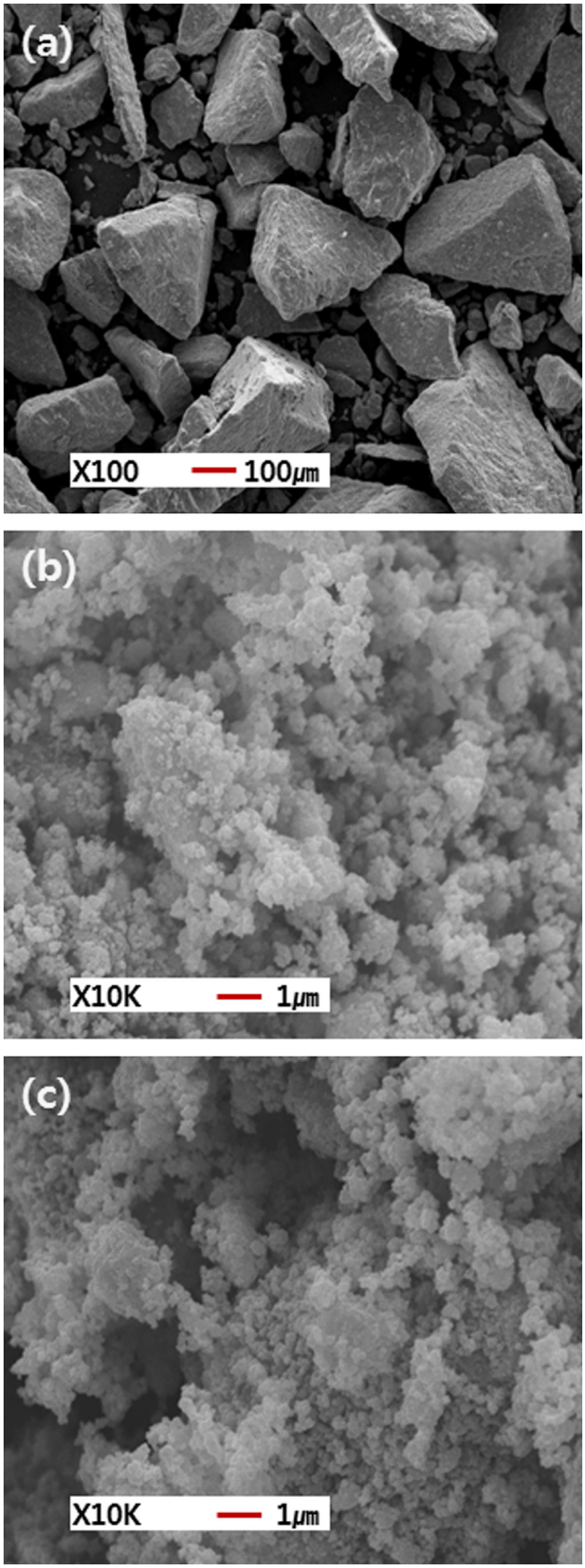

Fig. 3. SEM images of the milled Ti–Cr+graphite powder: (a) 0 h, (b) 10 h, and (c) 20 h.

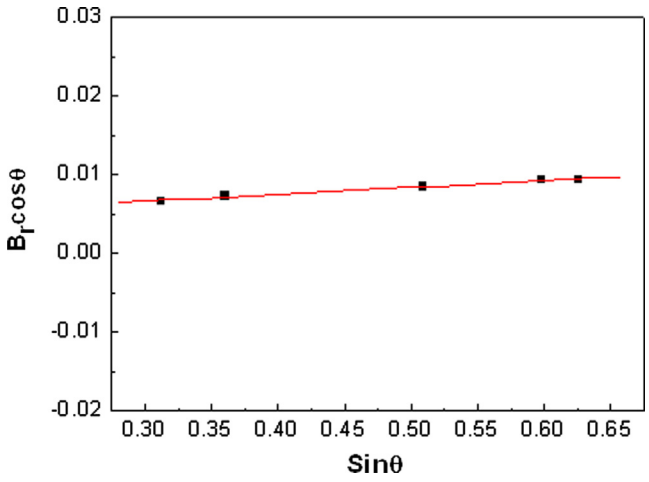

Fig. 4. Plot of $B_r(B_{crystalline}+B_{strain})\cos\theta$ versus $\sin\theta$ for (Ti,Cr)C powder synthesized via milling for 20 h.

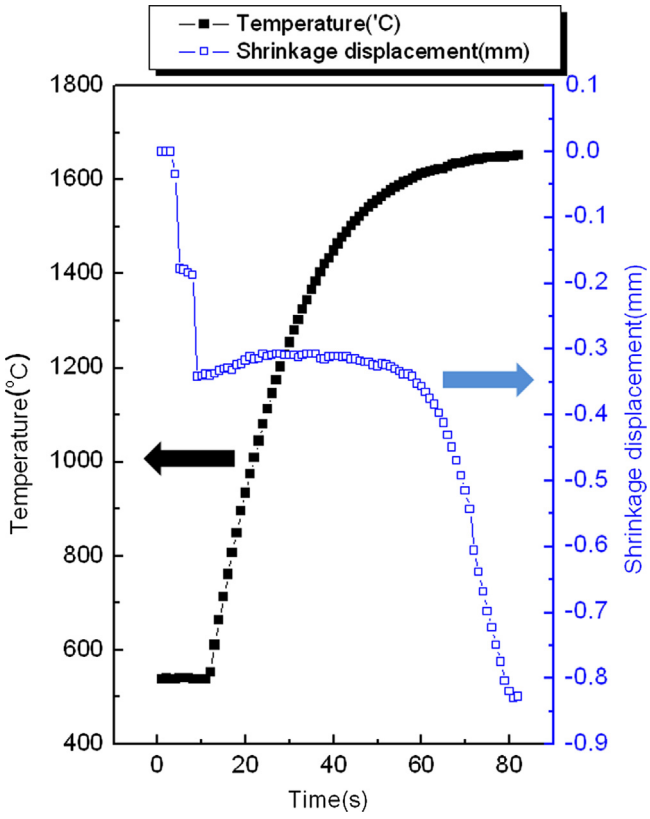

Fig. 5. Variations in temperature and shrinkage with heating time during the sintering of binderless (Ti,Cr)C powder.

Vickers hardness measurements were performed on polished sections of the (Ti,Cr)C samples using a 30 kg_f load and 15 s dwell time. Indentations with sufficiently large loads produced median cracks near the indent. The lengths of these cracks allow for the estimation of the fracture toughness of the materials [23]:

$$K_{IC} = 0.203(c/a)^{-3/2}H_v a^{1/2}, \quad (2)$$

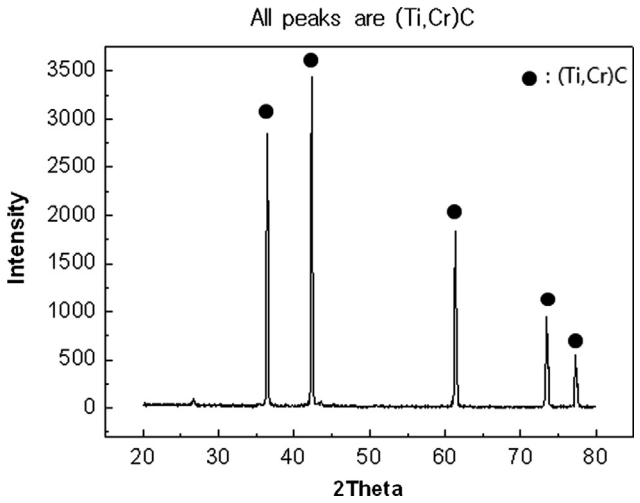

Fig. 6. XRD patterns of binderless (Ti,Cr)C sintered at 1650 °C.

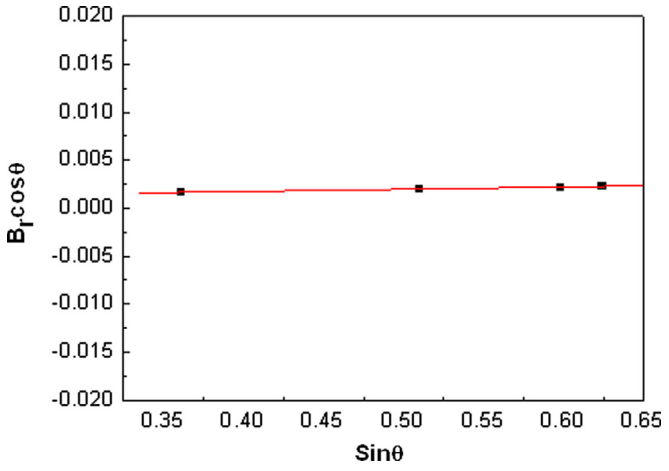

Fig. 7. Plot of $B_r(B_{crystalline}+B_{strain})\cos\theta$ versus $\sin\theta$ (Eq. (1)) for (Ti,Cr)C sintered at 1650 °C.

where c is the length of the crack measured from the center of the indentation, a is one-half of the average length of the two indent diagonals, and H_v is the hardness. The Vickers hardness and fracture toughness of the (Ti,Cr)C with ball milling for 20 h were 2068 kg/mm^2 and 7.8 MPa m$^{1/2}$, respectively. These values represent the average of five measurements.

TiC powder can be synthesized by self-propagating high temperature synthesis (SHS) [24], mechanical alloying (MA) [25,4], and electrothermal combustion [26]. The use of plasma activated sintering to consolidate mechanically alloyed TiC powder has been demonstrated by El-Eskandarany [4]. The mechanically synthesized nanopowder of TiC with an average grain size of 5 nm was consolidated at 1963 K for 5 min under a pressure of 38.2 MPa to a fully dense nanocrystalline TiC with an average grain size of 60 nm. Comparing the above study with the present, the sintering temperature and time of the high-frequency induction heated sintering are lower and shorter, respectively than those of plasma activated sintering. The fracture toughness (7.8 MPa m$^{1/2}$) of (Ti,Cr)C in this study is higher than that of monoclinic TiC [2]. Fig. 9 shows (a) Vickers hardness indentation and (b) median crack propagation of (Ti,Cr)C sintered at 1650 °C. Cracks emanate

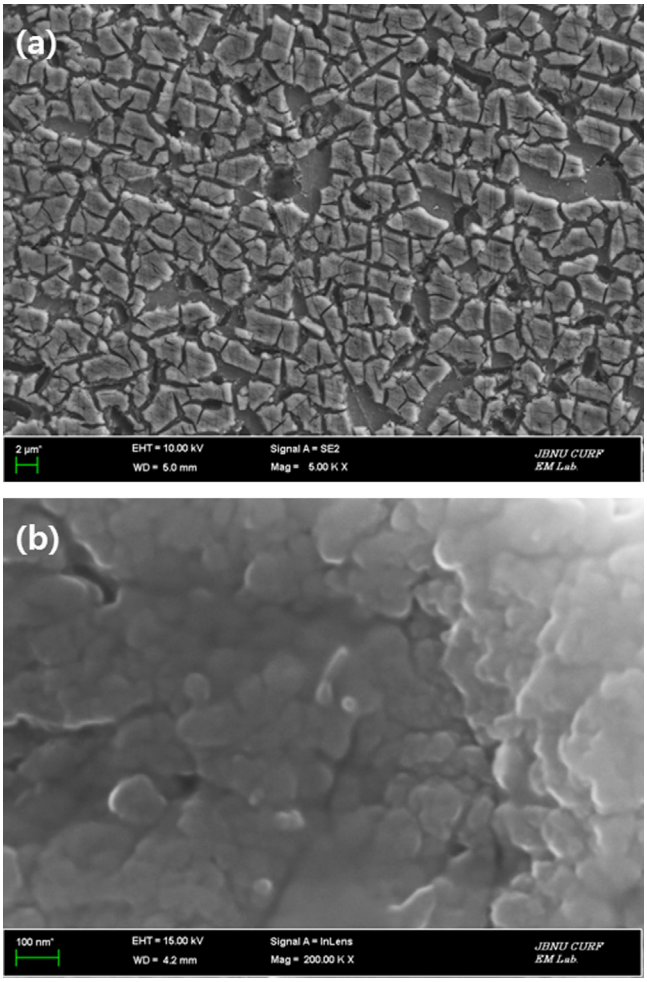

Fig. 8. FE-SEM micrographs of (Ti,Cr)C sintered at 1650 °C: (a) low magnification and (b) high magnification.

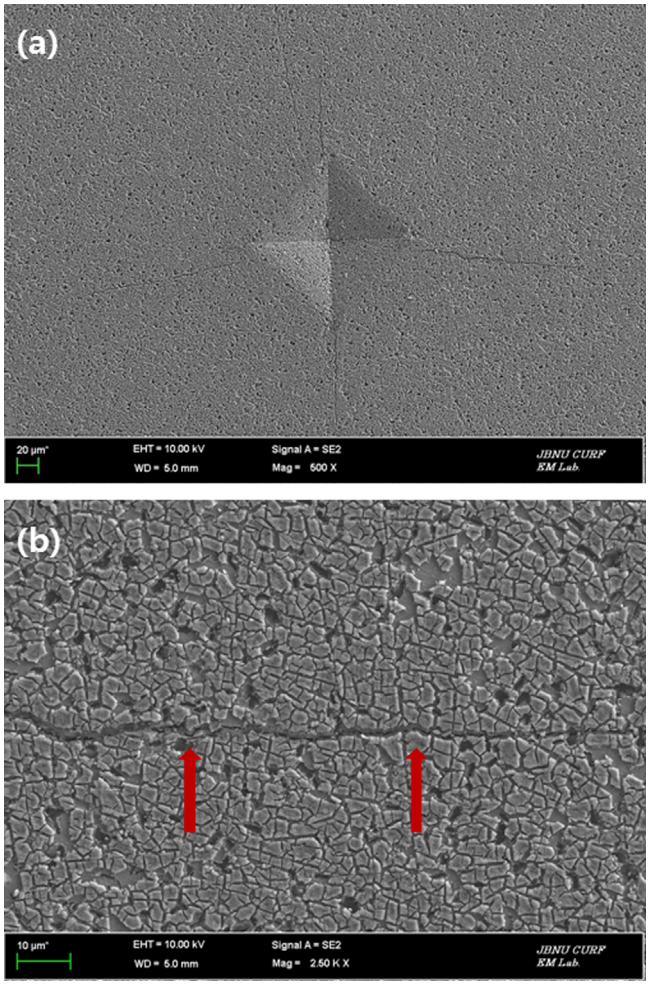

Fig. 9. (a) Vickers hardness indentation and (b) median crack propagating of (Ti,Cr)C sintered at 1650 °C.

from the corners of the indent in Fig. 9a. A higher magnification view of the indentation median crack in a (Ti,Cr)C sample is shown in Fig. 9b, which also shows that the crack has propagated in a perpendicular direction.

4. Summary

Nanocrystalline solid-solution carbide (Ti,Cr)C with nano-sized crystallites was prepared via the high-energy milling of Ti–Cr alloys with graphite. Using the new rapid sintering HFIHS method, densification of binderless (Ti,Cr)C was accomplished using high-energy ball milling. The average grain size of the (Ti,Cr)C was 150 nm, and the corresponding relative density was approximately 97%, for samples with milling times of 20 h. The Vickers hardness and fracture toughness of the (Ti,Cr)C were 2068 kg/mm^2 and 7.8 MPa m$^{1/2}$, respectively. The fracture toughness of (Ti,Cr)C was higher than that of monoclinic TiC.

Acknowledgments

This research was supported by the Basic Research Project of the Korea Institute of Geoscience and Mineral Resources (KIGAM), funded by the Ministry of Knowledge Economy of Korea, and by the Human Resources Development of the Korea Institute of Energy Technology Evaluation and Planning (KETEP) Grant funded by the Korea Government Ministry of Knowledge Economy (No. 20114030200060).

References

[1] I.J. McColm, N.J. Clark, High Performance Ceramics, Blackie Press, London, 1986.
[2] In-Jin Shon, Byung-Ryang Kim, Jung-Mann, Jin-Kook Yoon, Consolidation of binderless nanostructured titanium carbide by high-frequency induction heated sintering, Ceramics International 36 (2010) 1797–1803.
[3] In-Yong Ko, Na-Ra Park, Se-Hoon Oh, In-Jin Shon, Mechanical properties and fabrication of nanostructured (Ti,Mo)Si_2 by pulsed current activated combustion, Korean Institute of Metals and Materials 49 (2011) 608–613.
[4] M. Sherif El-Eskandarany, Structure and properties of nanocrystalline TiC full-density bulk alloy consolidated from mechanically reacted powders, Journal of Alloys and Compounds 305 (2000) 225–238.
[5] L. Fu, L.H. Cao, Y.S. Fan, Two-step synthesis of nanostructured tungsten carbide–cobalt powders, Scripta Materialia 44 (2001) 1061–1068.
[6] K. Niihara, A. Nikahira, Advanced Structural Inorganic Composite, Elsevier Scientific Publishing Co., Trieste, Italy, 1990.

[7] S. Berger, R. Porat, R. Rosen, Nanocrystalline materials: a study of WC-based hard metals, Progress in Materials 42 (1997) 311–320.
[8] Z. Fang, J.W. Eason, Study of nanostructured WC–Co composites, International Journal of Refractory Metals and Hard Materials 13 (1995) 297–303.
[9] A.I.Y. Tok, L.H. Luo, F.Y.C. Boey, Carbonate Co-precipitation of Gd_2O_3-doped CeO_2 solid solution nano-particle, Materials Science and Engineering A 383 (2004) 229–234.
[10] H.S. Kang, I.Y. Ko, J.K. Yoon, J.M. Doh, K.T. Hong, I.J. Shon, Properties and rapid low-temperature consolidation of nanocrystalline Fe–ZrO_2 composite by pulsed current activated sintering, Metals and Materials International 17 (2011) 57–62.
[11] F. Charlot, E. Gaffet, B. Zeghmati, F. Bernard, J.C. Liepce, Mechanically activated synthesis studied by X-ray diffraction in the F–Al system, Materials Science and Engineering A 262 (1999) 279–288.
[12] I.J. Shon, K.I. Na, I.Y. Ko, J.M. Doh, J.K. Yoon, Effect of $FeAl_3$ on properties of (W,Ti)C–$FeAl_3$ hard materials consolidated by a pulsed current activated sintering method, Ceramics International 38 (2012) 5133–5138.
[13] I.J. Shon, G.W. Lee, J.M. Doh, J.K. Yoon, Effect of milling on properties and consolidation of TiO_2 by high-frequency induction heated sintering, Electronic Materials Letters 9 (2013) 219–225.
[14] J. Jung, S. Kang, Sintered (Ti,W)C carbides, Scripta Materialia 56 (2007) 561–564.
[15] N.R. Kim, S.W. Cho, W. Kim, I.J. Shon, Fabrication of nanostructured Ti from Ti and TiH_2 by rapid sintering and its mechanical properties, Korean Journal of Metals and Materials 50 (2011) 34–38.
[16] I.J. Shon, I.Y. Ko, H.S. Kang, K.T. Hong, J.M. Doh, J.K. Yoon, Rapid synthesis and consolidation of nanostructured Al_2O_3–$MgSiO_3$ composites by high frequency induction heated sintering, Metals and Materials International 18 (2012) 109–113.
[17] I.Y. Ko, N.R. Park, I.J. Shon, Fabrication of nanostructured $MoSi_2$–$TaSi_2$ composite by high-frequency induction heating and its mechanical properties, Korean Journal of Metals and Materials 50 (2012) 369–374.
[18] Z. Shen, M. Johnsson, Z. Zhao, M. Nygren, Spark plasma sintering of alumina, Journal of the American Ceramic Society 85 (2002) 1921–1927.
[19] J.E. Garay, U. Anselmi-Tamburini, Z.A. Munir, S.C. Glade, P. Asoka-Kumar, Electric current enhanced defect mobility in Ni_3Ti intermetallic electric current enhanced defect mobility in Ni_3Ti intermetallics, Applied Physics Letters 85 (2004) 573–575.
[20] J.R. Friedman, J.E. Garay, U. Anselmi-Tamburini, Z.A. Munir, Modified interfacial reactions in Ag–Zn multilayers under the influence of high DC currents, Intermetallics 12 (2004) 589–597.
[21] J.E. Garay, J.E. Garay, U. Anselmi-Tamburini, Z.A. Munir, Enhanced growth of intermetallic phases in the Ni–Ti system by current effects, Acta Materialia 51 (2003) 4487–4495.
[22] C. Suryanarayana, M. Grant Norton, X-ray Diffraction: A Practical Approach, Plenum Press, New York, 1998.
[23] K. Niihara, R. Morena, D.P.H. Hasselman, Evaluation of KIC of brittle solids by the indentation method with low crack-to-indent ratios, Journal of Materials Science Letters 1 (1982)12-16 1 (1982).
[24] S.K. Mishra, S. Das, R.P. Goel, P. Ramachandrarao, Self-propagating high temperature synthesis (SHS) of titanium carbide, Journal of Materials Science Letters 16 (1997) 965–967.
[25] Q. Yuan, Y. Zheng, H. Yu, Mechanism of synthesizing nanocrystalline TiC in different milling atmospheres, International Journal of Refractory Metals and Hard Materials 27 (2009) 696–700.
[26] I.J. Shon, Z.A. Munir, Synthesis of TiC, TiC–Cu composites, and TiC–Cu functionally graded materials by electrothermal combustion, Journal of the American Ceramic Society 81 (1998) 3243–3248.